Int. J. Electrochem. Sci., 10 **(2015)** 7754 - 7770

International Journal of
ELECTROCHEMICAL
SCIENCE
www.electrochemsci.org

Field Studies of Corrosion Behaviour of printed circuit board and hot air solder levelling During the Marine Environment of Industrial Pollution

Pan Yi[1], *Kui Xiao*[1,2,*], *Chaofang Dong*[1,2], *Kangkang Ding*[1], *Ming Liu*[1], *Xiaogang Li*[1,2]

[1] Corrosion and Protection Center, University of Science and Technology Beijing, Beijing 100083, China
[2] Institute of Advanced Materials and Technology, University of Science and Technology Beijing, Beijing 100083, China
[*]E-mail: xiaokui@sina.com

Received: 11 May 2015 / *Accepted:* 26 June 2015 / *Published:* 28 July 2015

The atmospheric corrosion behaviour of PCB-HASL (electronic materials) in a polluted marine atmosphere environment was investigated by stereology microscope, SEM, EIS, XPS and SKP. It was found that deposition of chloride ions and SO_2 gas played a pivotal role in atmospheric corrosion, which contributed to an obvious undulation of the corrosion rate. In the late exposure test, the expansion of the corrosion products gave rise to the abscission of the protective coating layer (Sn), which resulted in substrate Cu directly exposing to atmospheric environment of Xiaomai Island and causing the Cu gradually corrosion.

Keywords: PCB-HASL; atmospheric corrosion; XPS; EIS

1. INTRODUCTION

With the continuous reform of electronic technology, the printed circuit boards (PCBs) as the electronic components are developing towards further miniaturization and highly integrated direction [1-2]. The deficiencies for these technological advances are that the electronic components become more sensitive to moisture and pollutants and still further liable to failures due to corrosion [3-4]. Typically, in order to enhance the ability of corrosion resistance and weldability of PCBs, a variety of surface coating treatments are adopted, such as immersion tin. However, lead-containing alloys have been banned from electronic and microelectronic products by the environmental protection agencies (RoHS and WEEE) [5-7]. As the legislation prohibiting and confining the use of the conventional Sn-

Pb alloys on PCBs [6-9], the process of lead-free tin hot air leveling (HASL) became one of the main surface treatments for printed circuit board due to superior weldability, excellent conductivity and environmental friendly [7,10]. In recent years, as the development and utilization of marine resources, more and more electronic equipment were used in the marine environment. Unfortunately, they are highly sensitive to corrosion in marine atmosphere with high Cl^- deposition rate, humidity, temperature and other pollutants. Hence, the effects of atmospheric on the corrosion processes of PCB should not be neglected, especially in some areas that are severely contaminated by SO_2. And the knowledge of corrosion mechanism of PCB-HASL in polluted marine atmosphere environment is necessary and imperative to supply the guidance for PCBs applications.

Lately, some researchers conducted a number of researchs anenst the corrosion behavior of PCB-HASL in various environments by employing laboratory simulation experiments [4,11-15]. Laboratory experiments are particularly important for the investigation of the corrosion mechanisms and elaborating the effects of specific pollutants and ions on the PCB-HASL. Zhong et al. [16] investigated the corrosion of Sn under thin electrolyte film containing Cl^- by electrochemical techniques and surface characterization and found that the corrosion products gradually became integral as the exposure time progressed, which can provide excellent protective performance, leading to the reducing of corrosion rate of Sn. Afterwards, Zou et al. [17] discussed the corrosion behavior of 63Sn-37Pb solder joint in wet H_2S environment and demonstrated that there was presence of the electrochemical migration (ECM) on tin-lead solder joints, and a Sn-rich phase with a more negativer electrode potential was corroded as anode. In recent years, Minzari et al. [4] and Zhong et al [11] described in detail the ECM mechanism of Sn. It concluded that ECM is mainly affected by the following factors: the ionic species in solution, inter-electrode distance and potential etc. by altering ionic migration, the electric field, stability of tin ions in solution, and kinetics of electrochemical reactions.

In the real field exposure, the synergetic influences of diversified factors involving Cl^- deposition rate, relative humidity (RH), SO_2 and temperature has an important influences on the corrosion of metals [18-21]. It is virtually impossible to simulate actual field exposure conditions using salt spray experiment, damp heat experiment and other accelerated tests [21], while very few studies have been carried out to the atmospheric corrosion of PCB-HASL in the field.

In this paper, in order to supply the fundamental insight on the corrosion behavior of PCB-HASL under the synergetic effect of SO_2, Cl^- and other particle deposition and provide a basis for the optimization of material selection and prevent failure happening, the corrosion behavior of PCB-HASL exposed in Xiaomai Island, Qingdao City, China, where the atmospheric environment is polluted severely by SO_2, for 12 months was investigated.

2. EXPERIMENTAL

2.1 Materials

The raw material, PCB-HASL, used in this work was from Sprine Co. in China. The basic parameters of PCB-HASL were shown in Table 1. And the schematically of PCB-HASL was shown in

Fig.1. Prior to the exposure tests, all the specimens were degreased by acetone followed by cleaning in distilled water. In order to better simulate the corrosion behavior of PCB-HASL in the polluted marine atmosphere, all the specimens were installed on a box (Fig.1) which were placed on a test rack in Xiaomai Islands (36°03′N, 120°25′E), Qingdao, China. Inside the box the PCB samples are fixed on the angle irons through the screw. The exposure lasted for 12 months (March 2014–March 2015). Six replicate samples were recovered from Xiaomai Island after 1, 3, 6, 9 and 12 months. Three replicas were used to determine the electrochemical test, and the other was employed to analyze the corrosion products and corrosion morphology.

Table 1. Basic parameters of PCB

M_{board}	T_{board}	T_{copper}	S	$T_{pro-layer}$
FR-4	0.8 mm	35 μm	HASL	1 μm

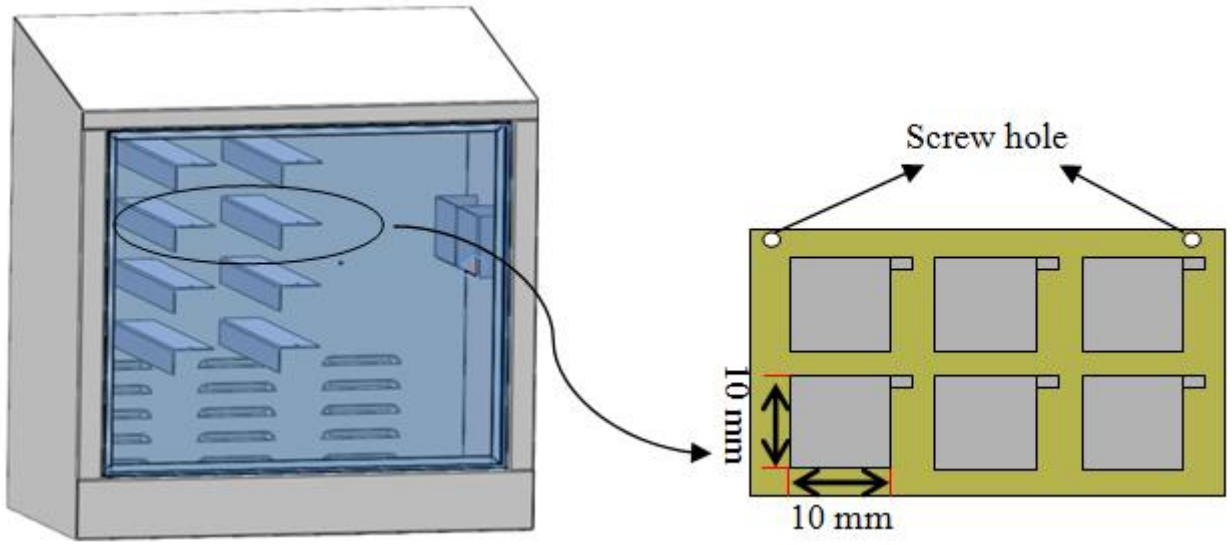

Figure 1. The schematically of PCB-HASL and the box

2.2 Environmental characteristics of exposure sites

The environmental characteristics, atmospheric pollutants measured at Xiaomai Islands and atmosphere classifications based on ISO9223 [22] were listed in Table 2. The relative humidity (RH) and average temperature in marine atmosphere of Xiaomai Island were 71% and 12.5 ℃, respectively. The time of wetness (TOW), namely, the period which a metallic surface was covered by adsorptive and/or a layer of electrolyte, was calculated as the length of time when RH was higher than 80% at a temperature greater than 0 ℃ [22]. The TOW of Xiaomai Islands among exposure experiments was 4049 h/year which geared to the classification of ζ4. The annual average deposition rate of Cl^- was 0.25 mg/(100cm^2·d), which geared to the classification of S1. In addition, the precipitation of SO_2 was

up to 1.184 mg/(100 cm^2·d), which was belonged to the classification of P3. It was stressed that the pH value located between 4 and 5.

Table 2. Environment characteristics of Xiaomai Islands

Location	Average temperature(℃)	Average RH	TOW (h/year)	Rain (mm/year)	Cl^- deposition rate mg/(100cm^2·d)	SO_2 deposition rate mg/(100cm^2·d)	Average pH
Xiaomai Islands	12.5	71	4049	643	0.25	1.184	4.58

2.3 Corrosion products analysis

Macro-morphologies of specimens after exposure test were recorded by stereology microscope (KEYENCE VHX2000). Micro-morphologies and EDS analysis of corrosion products on the surfaces of PCB-HASL were detected by FEI Quanta 250 environment scanning electron microscope. Moreover, the corrosion products were analyzed by X-ray photoelectron spectroscopy (XPS). XPS test was carried out using Thermo ESCALAB 250Xi with an Al Ka (1486.6 eV) X-ray source. The binding energy was adjusted for charging effect by referencing to the C1s peak (284.8 eV). Registered core-level spectra were fitted to mixed Gaussian–Lorentzian lineshapes according to Shirley-type background subtraction by XPSPEAK v4.1 software.

2.4 Electrochemical tests

Electrochemical tests were carried out in a traditional three-electrode system by using a PARSTAT M2273 electrochemical workstation. The auxiliary electrode was a platinum foil and the reference electrode was a saturated calomel electrode (SCE). EIS measurements were carried out at open circuit potential with a perturbation of 10 mV and the measuring frequency ranged from 100 kHz to 10 mHz with 5 points per decade. All of the electrochemical measurements were performed after 30 min immersion of the specimens in 0.1 M Na_2SO_4 solution. All electrochemical tests were repeated three times to ensure their reproducibility of the measurements. The fitting of EIS has been done by ZSimpWin software.

2.5 SKP measurements

The method of SKP measurements is based on an alternative current and capacitor between a metallic probe and a working electrode which were caused by the ceaseless vibration of the probe on top of the working electrode surface. The current is magnified and the external direct current bias is appended to compensate the signal. The direct current bias is in connection with the contact potential difference between the working electrode surface and the probe. This potential drop that is located in the air gap separating the probe and metal is corresponding to the difference in Volta potential of the

materials. Hence the potential difference and correspondingly the potential of the working electrode can be gained [23-25]. Further details about SKP measurements of PCB are given elsewhere [2,26].

In this paper, a M370 Scanning Probe Measurements System was used. A flat-ended cylindrical tungsten needle was employed as the probe, which was moved at three stepping motors for the x-, y- and z-. All areas were performed automated, while the distance of sample and probe was defined as 100±2 μm manually before starting scan. The step size was 100 μm /point in the X-axis direction and 50 μm /point in the Y-axis direction. The vibration amplitude and the frequency were 30 μm and 80 Hz, respectively. The needle potential was calibrated relatively to a $Cu/CuSO_4$ electrode before the experiment.

All the measurements experiments were operated in the laboratory environment of 20 ℃ and 40% RH.

3. RESULTS

3.1 Corrosion products analysis

3.1.1 Surface morphology

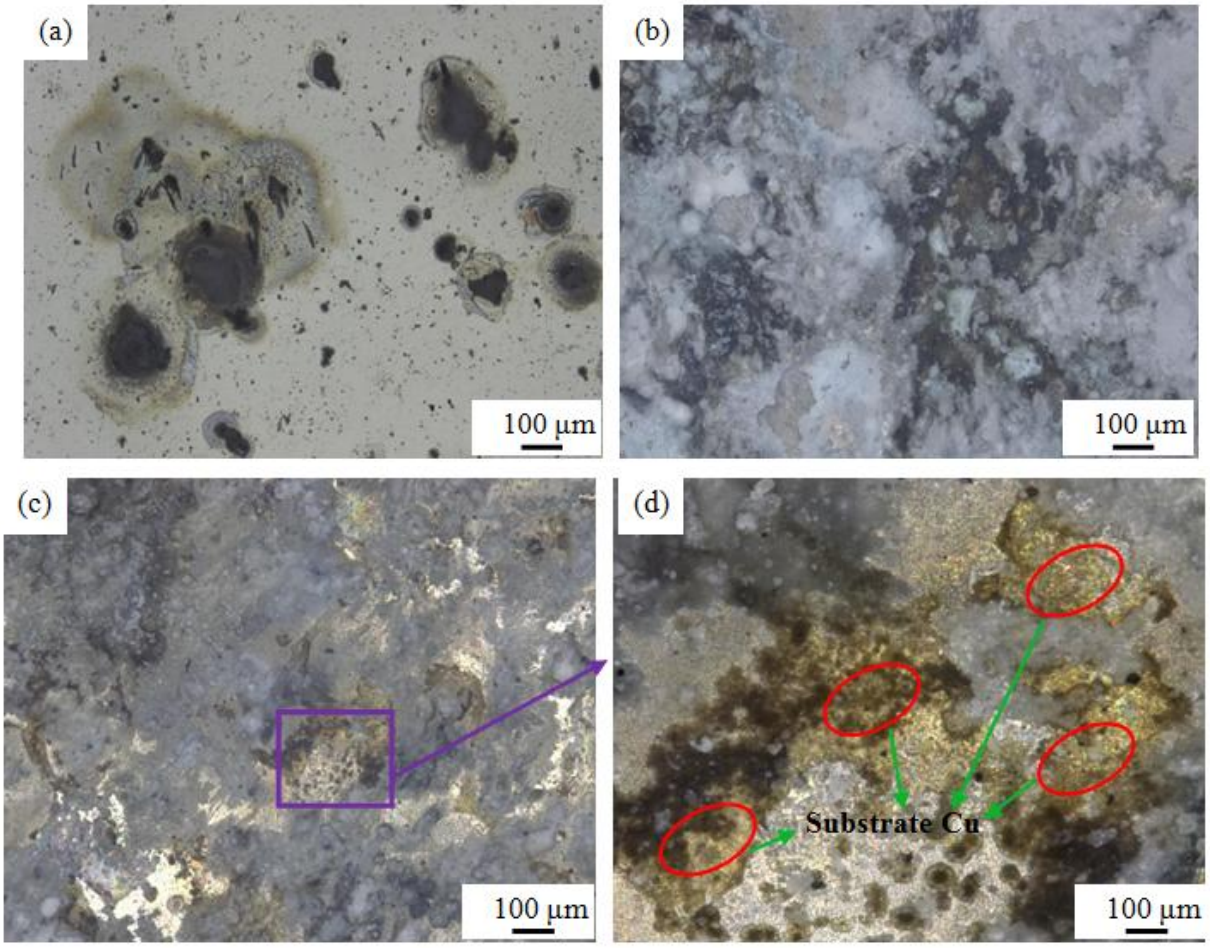

Figure 2. Macro-morphologies of the outdoor PCB-HASL samples exposed for different cycles (a) 1m; (b)6m; (c)12m; (d) selected area from (c)

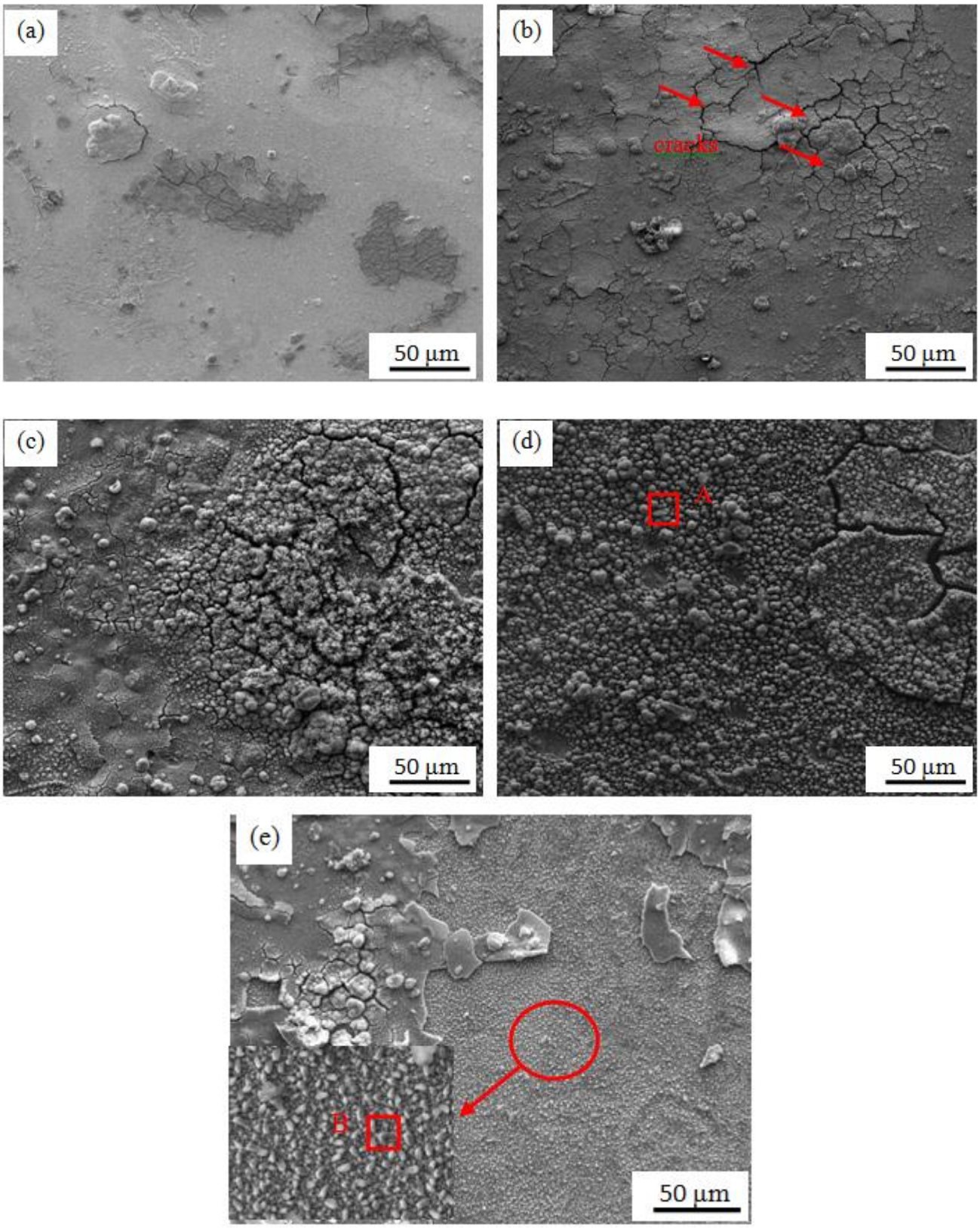

Figure 3. Micro-scopic morphologies of corrosion products formed on PCB-HASL under different exposure periods: (a) 1 m, (b) 3 m, (c) 6 m, (d) 9 m, (e) 12 m

Macro-morphologies photographs of the outdoor PCB-HASL samples are shown in Fig. 2. As can be seen from Fig. 2(a), the PCB-HASL samples corroded slightly at exposure 1 m, with localized discoloration areas dispersed on the sample surface in halo-like shape. It can be speculated that the center of discoloration area is where pitting corrosion occurred and the color change is mainly caused by the corrosion of local PCB-HASL. As time elapses (6 m), a number of corrosion products covered on the surface of PCB-HASL (Fig. 2(b)). Up to 12 m, there was presence of dark yellow corrosion products (Fig. 2(c)). Enlarged in the local region, it found that the surface protective coating layer shed, which resulted in Cu substrate directly exposing to the atmosphere, as was shown Fig. 2(d).

Fig. 3 shows the micro-scopic morphologies of the corrosion products formed on PCB-HASL after exposing for different periods. The images display the notable evolution of surface morphologies at various time. After 1 month of exposure, some local area of specimen became rough and some corrosion products were randomly distributed on the surface, which may be happened initially on the weakness sites of the surface oxide film (Fig. 3a). Three months later, there were a large number of cracks and voids on the surface of PCB-HASL, which were mainly ascribed to the dehydration reaction during wet-dry cycles (Fig. 3b). As the exposure time progressed, corrosion product gradually increased (Fig. 3(c-d)). The EDS mapping analysis of the A area on PCB-HASL showed the oxygen content was higher in the corrosion products, while Cu was little on the area. This indicated that the corrosion product was mainly the compound of Sn, as was listed in Table 3. After weathering for 12 months, there was presence of the cracking and shedding of large areas of corrosion products (Fig.3(e)). EDS analysis was carried out for the B area, it found that Cu content increased, which suggested that Cu has been directly exposed to atmospheric environment and the surface protective coating layer (Sn) has lost the protection role.

Table 3. The element contents in the corrosion products marked in Fig. 3 determined by EDS

Element	C	O	S	Cl	Sn	Cu	others
Area A, At%	5.48	49.93	1.23	0.89	35.67	1.14	5.66
Area B, At%	5.23	15.04	0.86	0.81	29.37	44.38	4.32

3.1.2 XPS analysis

Considering the detection limitation of EDS measurements in the element detection, in order to evaluate the chemical surface composition of corrosion product, a careful XPS investigation was conducted. Fig. 4 and Fig. 5 show high-resolution images of Sn 3d and Cu 2p spectra of corrosion product after 12 month of exposure.

From the Fig.4(a), we can see that the Sn 3d peak is asymmetrical and wide, which indicates the presence of multiple oxidizing states of Sn in the corrosion product. It is fitted with a doublet representing spin orbit splitting of Sn 3d5/2 and Sn 3d3/2 peaks. And the core-level Sn 3d5/2 spectrum is deconvoluted into three peaks at 486, 486.6 and 487.4 eV. The ellipse area in Fig.4(a) is attributed to

the higher back bottom which was deducting. Peaks detected at 486 and 486.6 eV are respectively attributed to SnO and SnO_2 [16,27], and peaks detected at 487.4 eV are attributed to $SnCl_2$ [28].

Fig. 4(b) shows high-resolution XPS spectrum of Cu 2p. It must be stressed that there were the presence of strong satellite peaks in XPS spectrum of Cu 2p, which illustrated that there is probably a component of CuO in the corrosion product layer [29,30]. Then a procedure of decomposition of XPS Cu 2p is performed, it is seen that three overlapping peaks correspond, one at 933.5 eV (CuO) [31], one at 934.4 eV ($CuCl_2$) [32] and another at 935.5 eV ($CuSO_4$) [33].

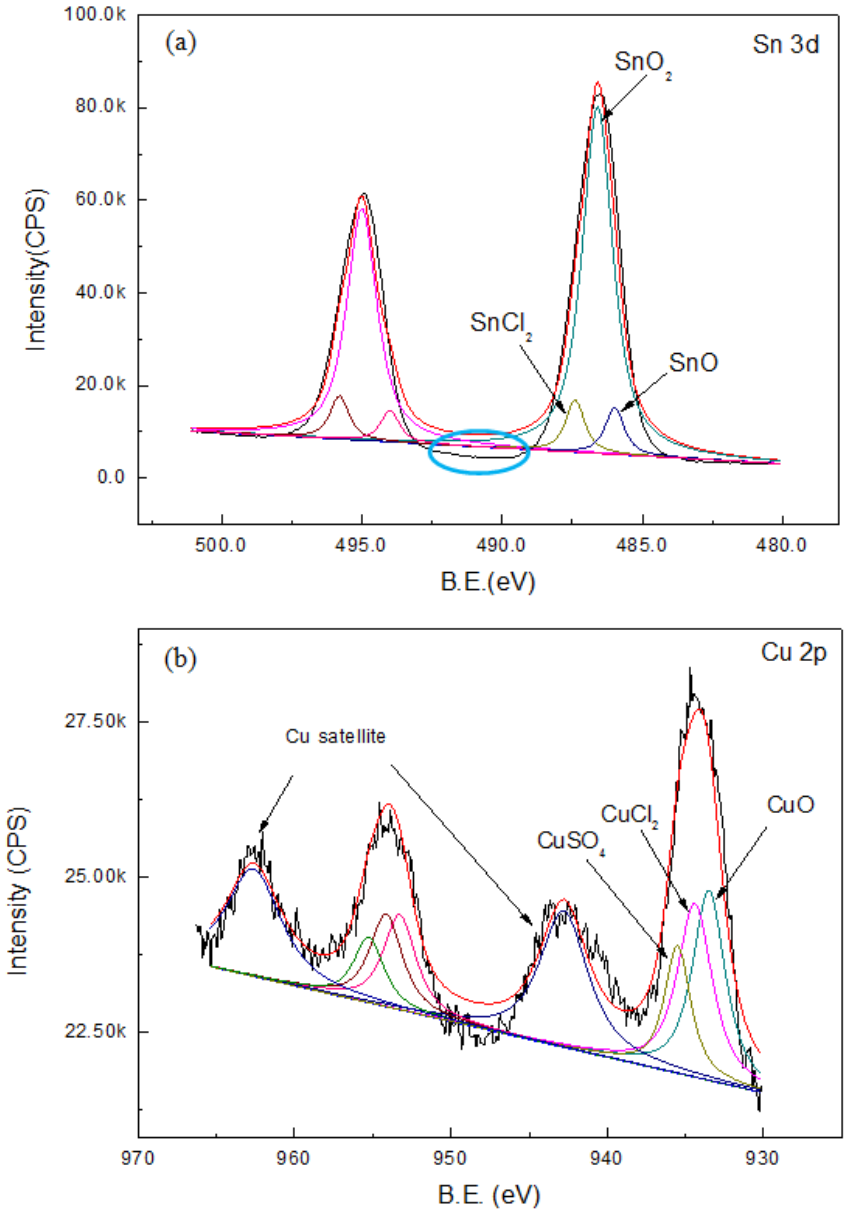

Figure 4. The high-resolution spectrum of the corrosion products formed on PCB-HASL: (a) Sn 3d; (b) Cu 2p

3.2 Electrochemical measurements

Except for environmental atmosphere factors, the corrosion products covered on metals have vital influence on corrosion process [34-36]. The protection ability of corrosion products were determined by their compactness, solubility, chemical composition, conductivity, morphology and hygroscopicity [21]. It was seen that, in Fig. 3, corrosion products of PCB-HASL showed different features after exposure for different periods.

The Nyquist and Bode diagrams obtained for the PCB-HASL at OCP in 0.1 M Na_2SO_4 solution are presented in Figs. 5 and 6, respectively. For 1 m-9 m exposure test, it seemed that there was only one capacitive semicircle in the Nyquist plot from Fig. 5, i.e. one time constant. But the Bode plots showed that there were two time constants, as was shown in Fig.6. Thus the equivalent electrical circuit was given in Fig.7(a) was used to fit the EIS of the PCB-HASL to explicate the corrosion behaviour. For 12 m exposure test, there was three time constant in the Bode. Consequently, to gain the electrochemical parameters, the equivalent circuit (EC) in Fig. 7 (b) was employed to fit the EIS data of PCB-HASL. R_s was the solution resistance and high-frequency circuit CPE_f-R_f corresponded to the capacitance and resistance of outer corrosion product (tin corrosion products); CPE_h-R_h related to the capacitance and resistance of inner corrosion product (copper corrosion products); medium-low frequency circuit R_{ct}-CPE_{dl} was the double-layer capacitance and charge transfer resistance.

In the circuit model (Fig. 7), instead of capacitance, constant phase elements (*CPE*) were used in the fitting process. The impedance of the CPE is given by Eq. (1),

$$Z_{CPE} = \frac{1}{Y_0(j\omega)^n} \quad (1)$$

where Y is a parameter related to capacitance, ω is the angular frequency and n is corresponding to non-uniform current distribution due to surface heterogeneity and roughness [37-39].

Table 4 summarized the values of circuit elements for PCB-HASL obtained by fitting of the EIS data. As it can be observed, comparing the results obtained for PCB-HASL, the value of the capacitance (CPE_{dl}) is varied between 10 and 90 $\mu F \cdot cm^{-2}$ in the first 9 months of exposure period. However, according to investigations, the capacitance of double-layer is approximately 60 $\mu F \cdot cm^{-2}$ for the smooth electrode [39-40]. The main reason is that the real area of the PCB-HASL is varied in the corrosion process, which caused the deviation from the smooth electrode. It must be noted that CPE_{dl} value (493 $\mu F \cdot cm^{-2}$) at 12 m was considered too high for a double layer, which may be explained by the influence of low pH resulted from the high concentration of SO_2 in Xiaomai Island. In fact, the capacitance is found to show a minimum for pH close to 6, increasing exponentially as the pH decreases [41]. Moreover, with the extension of exposure period, the n value of the electrical double layer decreased gradually. This phenomenon can be elaborated as follows: the products-covered samples progressively augmented as exposure time elapses, which was resulted in the changing of surface roughness of PCB-HASL.

Fig. 8 shows that time dependence of $1/R_{ct}$ of PCB-HASL under different exposure cycles. It can be seen that the corrosion rates of PCB-HASL increased at the initial moment (1 m and 3 m), and with extending of the exposure time, reverse phenomena appeared on corrosion rate during exposure from 3 m to 9 m. However, the corrosion rate slightly increased again after exposure for 12 months.

This phenomenon can be expatiated as follows: at the beginning of the experiment, the PCB-HASL is covered by a layer of oxide film. Unfortunately, the chloride ion is capable of strong damage, especially in the environment containing SO_2 [42]. Therefore, at first, weak oxide film area was destroyed, and caused the corrosion rate increased. As the exposure time progressed, massive corrosion products formed on the surface of PCB-HASL, which hindered the electrochemical dissolution process (3 m-9 m). During the remaining of the experiment (9 m-12 m), corrosion rate increased which was resulted from the abscission of the protective coating layer (Sn).

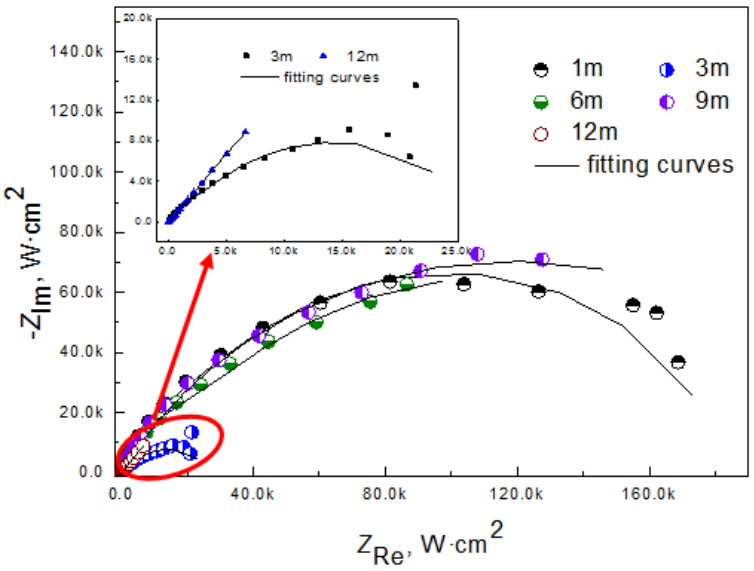

Figure 5. Nyquist diagram obtained for the PCB-HASL at OCP in Na_2SO_4 solution

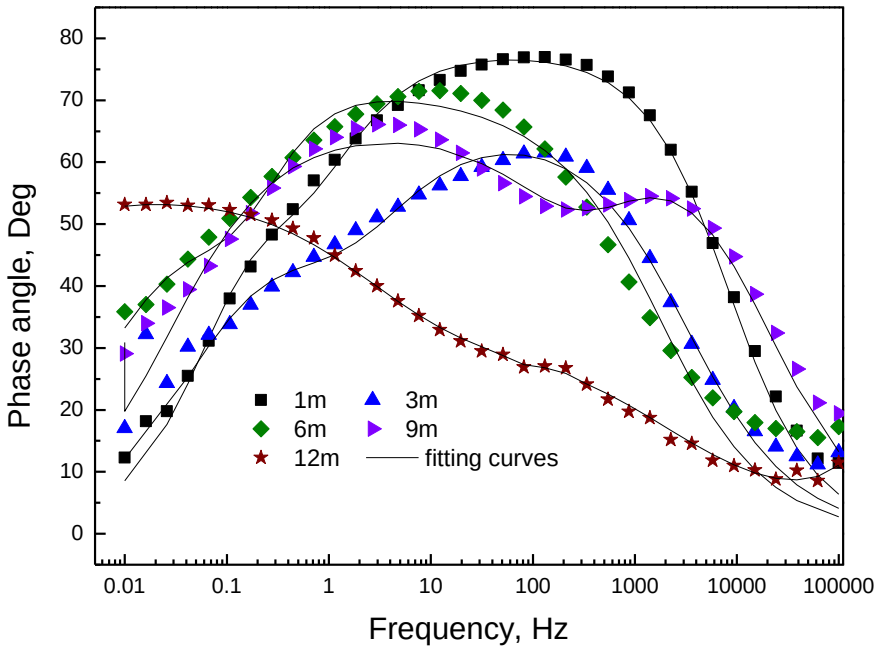

Figsure 6. Bode diagram obtained for the PCB-HASL at OCP in Na_2SO_4 solution

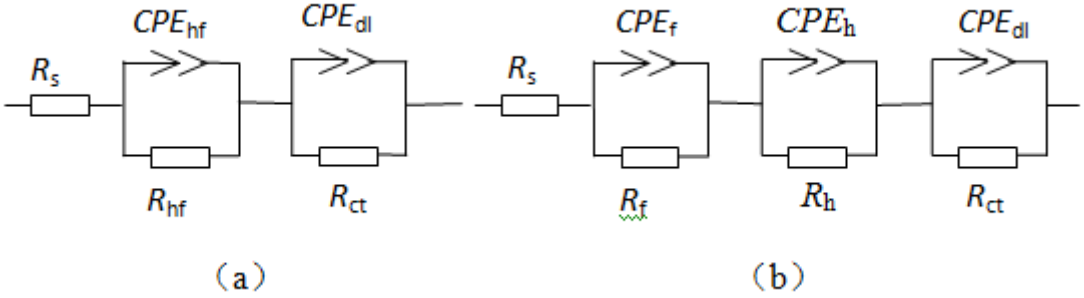

Figure 7. The equivalent circuits used for fitting EIS in Fig. 7

Table 4. The fitting results of EIS of PCB-HASL

cycle/h	R_s/(Ω·cm^2)	CPE_f / (S·s^n·cm^{-2})	n	R_f /(Ω·cm^2)	CPE_h / (S·s^n·cm^{-2})	n	R_h /(Ω·cm^2)	CPE_{dl} /(S·s^n·cm^{-2})	n	R_{ct} /(Ω·cm^2)
1	14.74	9.781E-6	0.8761	2.265E4	--	--	--	1.21E-5	0.8584	1.607E5
3	18.85	5.671E-5	0.7632	2143	--	--	--	8.579E-5	0.7127	2.467E4
6	25.36	5.084E-5	0.9616	1.407E4	--	--	--	4.738E-5	0.7261	2.008E5
9	13.76	3.243E-5	0.9886	3.347E4	--	--	--	3.261E-5	0.6244	3.324E5
12	35.61	5.601E-9	1	38.27	4.809E-4	0.4728	168.2	4.854E-4	0.6192	2.648E5

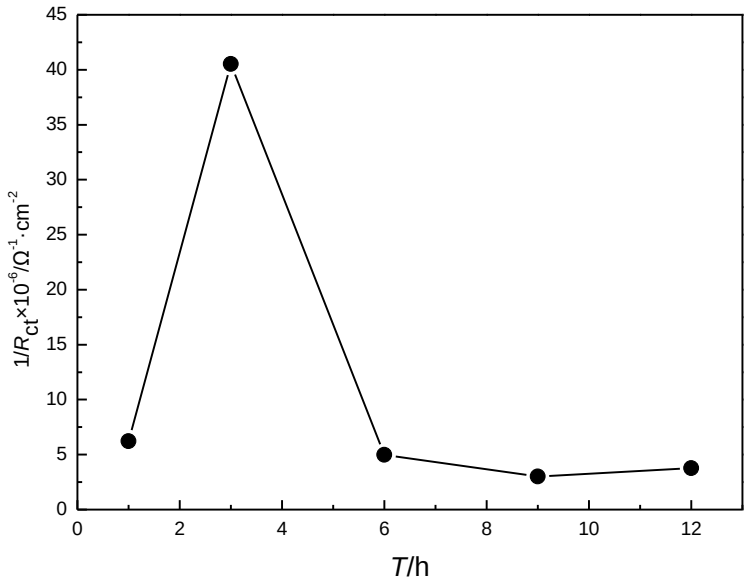

Figure 8. The time dependence of $1/R_{ct}$ under different exposure cycles

3.3 SKP surface characterization

Fig. 9(a-e) shows the potential distribution across the PCB-HASL during the different exposure periods. In order to better characterize the surface Kelvin potential distribution of corrosion products, Gauss fitting was carried on. Gauss fitting equation was shown in Eq. (2),

$$y = y_0 + \frac{A}{w\sqrt{2\pi}} \exp\left(-\frac{(x-\mu)^2}{2w^2}\right) \qquad (2)$$

where μ is the expected value, i.e. the central location of potential distribution; σ=ω/2, is the standard deviation of the distribution of Gauss, that is, the discrete degree of potential distribution. The σ value is larger, the potential distribution is more dispersed [2,43].

The Gauss fitting curves and the corresponding parameters are shown in Fig. 9(f) and Table 5. It describes significant evolution of surface Kelvin potential at various periods. As can be seen, in the early exposure, the surface potential was lower and the discrete degree of potential distribution was grater, which led to the larger of corrosion tendency of PCB-HASL. Accordingly, the darker area, i.e. the anode area, suffered from preferential corrosion, where developed as the "pitting" source later. As time elapses (6 m), under the synergistic effect of chlorine and sulfur dioxide, surface Kelvin potential gradually increased to -0.09021 V due to a number of corrosion products covered on PCB-HASL. Moreover, the corrosion products film hindered the electronic escape process on the sample surface, resulting in the color of the entire potential map changing into a warm tone. However, after 9 month of exposure, pitting corrosion gradually evolved into general corrosion, surface potential tends to descend. The main reason was that the expansion and local shedding of the corrosion products, which led to the substrate Cu directly exposing in the atmosphere. In fact, the corrosion subsequently occurred on substrate Cu, which in turn caused the rise of the surface potential during the remaining of the experiment (12 m).

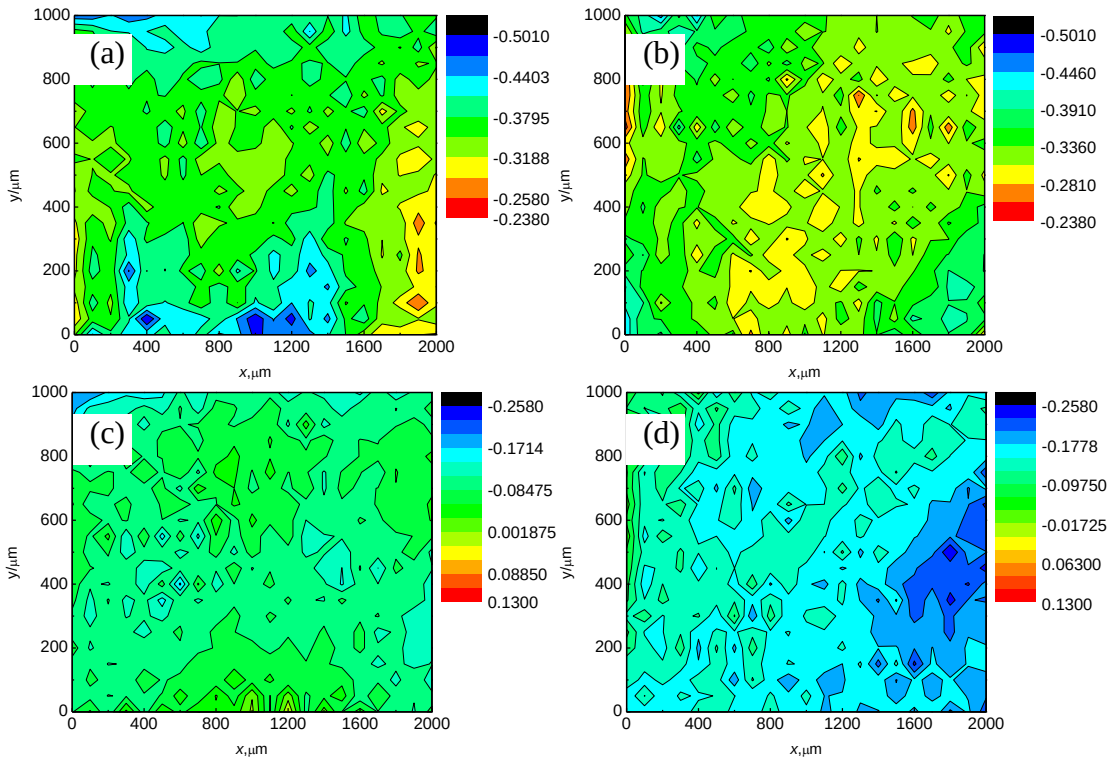

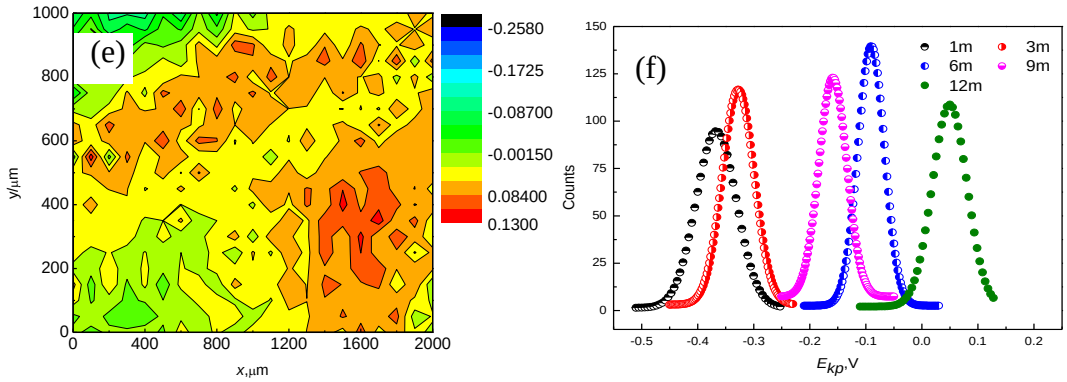

Figure 9. Surface SKP potentials distribution and Gauss fitting curves of PCB-HASL with different exposure time (a) 1 m; (b)3 m; (c)6 m; (d)9 m; (e)12 m; (f) Gauss fitting curves

Table 5. Gauss fitting results of surface SKP potentials distribution

	1m	3m	6m	9m	12m
μ,V	-0.3666	-0.32745	-0.09021	-0.15862	0.04967
σ	0.03602	0.0284	0.02377	0.02488	0.03102

3.4 Atmospheric corrosion behavior of PCB-HASL in the marine environment of industrial pollution

Based on the analysis of stereology microscope, SEM, EIS, XPS and SKP, a model for the corrosion of PCB-HASL under the actual atmospheric environment could be presented. The corrosion of PCB-HASL was initiated from pitting corrosion and then transformed into general corrosion with the exposure time prolonged. Fig. 10 was the schematic illustration of atmospheric corrosion of PCB-HASL under the combined effect of sulfur dioxide and chlorine ions.

A layer of thin electrolyte film emerged on the surface of specimen due to the strong hygroscopicity of sodium chloride that covered the PCB-HASL. It must be noted that SO_2 dissolved into the thin water film is known to become bisulfite (HSO_3^{2-}) ions by hydrolysis. Then, HSO_3^{2-} ions are further oxidized to SO_4^{2-} [44], as was shown in Eq. (3-5):

$$SO_2(g) \rightarrow SO_2(aq) \quad (3)$$

$$SO_2(aq) + H_2O \rightarrow HSO_3^- + H^+(aq) \quad (4)$$

$$HSO_3^-(aq) + 1/2O_2 \rightarrow SO_4^{2-} + H^+ \quad (5)$$

In fact, this also led to the low pH environment (acid rain) in Xiaomai Island, Qingdao. The reaction on the cathode under thin electrolyte layer may be the reduction of oxygen and hydrogen, as was shown in Eq. (6-7):

$$O_2 + 4e^- + 2H_2O \rightarrow 4OH^- \quad (6)$$

$$2H^+ + 2e^- \rightarrow H_2 \quad (7)$$

The anodic dissolution of tin is quite complicated. At the beginning of the exposure test, there existed a layer of oxide film on the surface of the PCB-HASL specimens. In this case, corrosion preferentially occurred in the site of weak oxidation film by the reaction (8-10) [2, 13], as was shown

in Fig. 10(a-b). Afterwards, the "fresh" Sn layer was dissolved by degrees under acid environment [13,45], as was shown in Eq. (11-13).

$$SnO_2 + 4H^+ \rightarrow Sn^{4+} + 2H_2O \quad (8)$$

$$SnO + 4H^+ \rightarrow Sn^{2+} + 2H_2O \quad (9)$$

$$SnO\ (SnO_2) + 2Cl^- \rightarrow SnCl_2\ (SnCl_4) \quad (10)$$

$$2Sn + 4H^+ + O_2 \rightarrow 2Sn^{2+} + 2H_2O \quad (11)$$

$$2Sn + O_2 + 2H_2O \rightarrow 2Sn(OH)_2 \quad (12)$$

$$2Sn(OH)_2 + O_2 + 2H_2O \rightarrow 2Sn(OH)_4 \quad (13)$$

In the meantime, a majority of $Sn(OH)_2$ and $Sn(OH)_4$ will further dehydrate and evolve as more stable tin oxide (SnO and SnO_2) as the reactions Eq. (14-15) [46],

$$Sn(OH)_2 \rightarrow SnO + H_2O \quad (14)$$

$$Sn(OH)_4 \rightarrow SnO_2 + 2H_2O \quad (15)$$

As the exposure time extended, local area of PCB-HASL was covered by corrosion products with massive cracks and voids. Remarkably, these areas gradually evolved as pitting. Moreover, the pits tended to spread laterally and the corrosion process is mostly controled by the formation of new pits and development of stable pits on the start stage [21], as was shown in Fig.10 (c).

However, after 9 month of exposure, some pits connected to each other which resulted in general corrosion. The volume of corrosion product (sulfate, oxides etc.) was much larger than that of the original, under the influence of alternating dry-wet and diurnal temperature difference, it led to cracking of corrosion product and the abscission of the protective coating layer (Sn layer). At this time, substrate Cu was directly exposed to atmospheric environment of Xiaomai Island. In an acidic environment, copper happened to dissolve in accordance with the formula 16-17 [47]. In fact, since the water content on the surface of the specimen was small, the dissolved Cu^{2+} were directly combination with SO_4^{2-} and Cl^- so that they reached saturation and crystallized (Eq. (18-19)) [48], as was shown in Fig. 10(d), which led to the corrosion products containing copper chloride and sulfide. In reality, in the aspect of thermodynamics, this also led to increasing in the surface potential of the sample, as shown in Fig.9(e).

$$Cu \rightarrow Cu_{ads}^{+} + e^- \quad (16)$$

$$Cu_{ads}^{+} \rightarrow Cu^{2+} + e^- \quad (17)$$

$$Cu^{2+} + 2Cl^- \rightarrow CuCl_2 \quad (18)$$

$$Cu^{2+} + SO_4^{2-} \rightarrow CuSO_4 \quad (19)$$

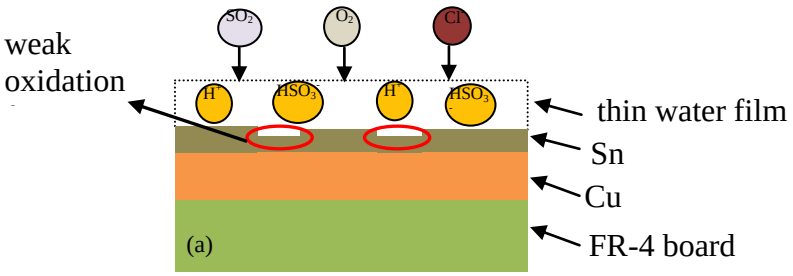

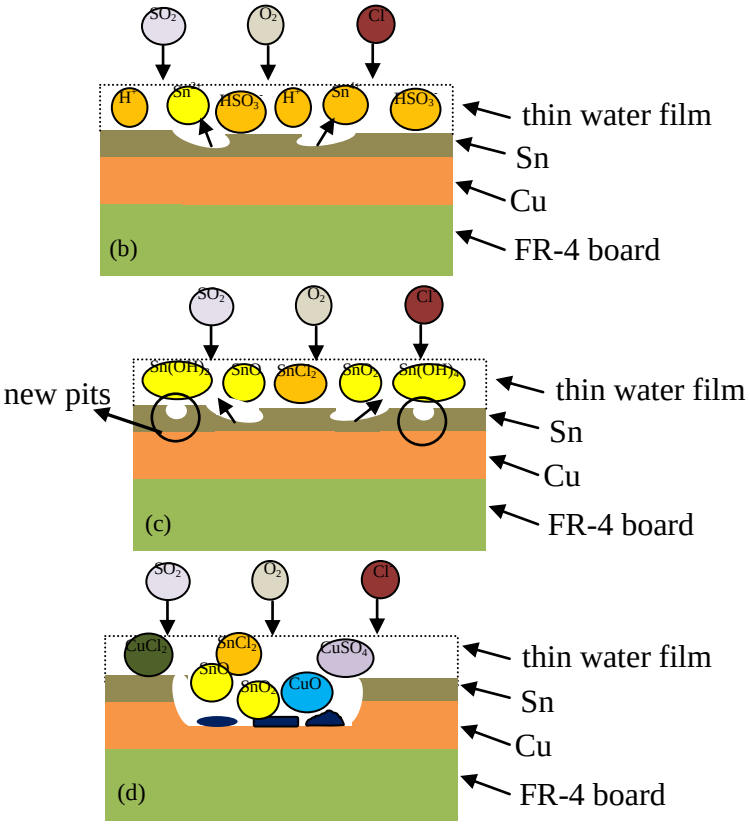

Figure 10. The schematic illustration of atmospheric corrosion of PCB-HASL

4. CONCLUSIONS

PCB-HASL was exposed to the marine environment of industrial pollution for 1 year, and the atmospheric corrosion behavior of the PCB-HASL was studied. The morphology of corrosion products were observed in detail with stereology microscope and SEM, the corrosion products were analyzed with EDS and XPS, and electrochemical process was discussed by EIS and SKP. Based on the analysis, a model for failure corrosion of PCB-HASL under marine environment of industrial pollution could be presented. The primary conclusions gained from this study are presented as follows:

(1) Corrosion pits initially occurred on PCB-HASL in marine environment of industrial pollution, which it evolved from pitting corrosion to general corrosion. Moreover, after 9 month of exposure, the surface protective coating layer (Sn) shed off due to the expansion of the corrosion products, which resulted in substrate Cu directly exposing to atmospheric environment of Xiaomai Island. Markably, there was presence of CuO, $CuCl_2$, $CuSO_4$ in corrosion product by XPS analysis, which demonstrated that the substrate Cu suffered corrosion. Moreover, the corrosion products tin included SnO, SnO_2 and $SnCl_2$.

(2) In the aspect of thermodynamics, Kelvin surface potential of the specimens gradually increased, anomaly occurs at 9 month. Large cracks and exposed “fresh” substrate (Cu) must be responsible for reducing of Kelvin potential. Later, corrosion of substrate contributed to increasing of Kelvin surface potential at 12 m.

(3) In the aspect of dynamics, during the process of field exposure test, the corrosion rate ($1/R_{ct}$) firstly enlarged, and then decreased after 3 month, and again suddenly augmented at 12 month. The main reason was that the corrosion product covered PCB-HASL restrained the corrosion process. However, the end of the experiment, the cracking and shedding of corrosion products caused a slight increase in corrosion rate instead.

ACKNOWLEDGEMENT
This research was supported by National Natural Science Foundation of China (51271032& 51131005) and the Major State Basic Research Development Program of China (973 Program: No. 2014CB643300).

References

1. K Kantola and R Tenno, *J. Mater. Process Tech.* 209 (2009) 2707-2714.
2. K K Ding, K Xiao, S W Zou, C F Dong, R T Zhao and X G Li, *Acta Metall. Sin*. 10 (2014) 1269-1278.
3. C Leygraf and T Graedel. *Atmospheric Corrosion*, New York: John Wiley&Sons, (2000).
4. D. Minzari, M. S. Jellesen, P. Møller and R. Ambat, *Corros. Sci.* 53 (2011) 3366-3379.
5. S. P. Yu, H. J. Lin and M. H. Hon, *J. Mater. Sci*. 11 (2000) 461-471.
6. R. A. Islam, Y. C. Chan, W. Jillek and S. Islam, *Microelectron. J*. 37 (2006) 705-713.
7. W. R. Osório, E. S. Freitas, J. E. Spinelli and A. Garcia, *Corros. Sci*. 80 (2014) 71-81.
8. L. R. Garcia, W. R. Osório, L. C. Peixoto and A. Garcia, *Mater. Charact*. 61 (2010) 212-220.
9. F. X. Che, W. H. Zhu, E. S. W. Poh, X. W. Zhang and X. R. Zhang, *J. Alloys Compd*. 507 (2010) 215-224.
10. C Harper. *Electronic Materials and Processes Handbook*, New York: McGraw-Hill, (2009).
11. X. Zhong, G. Zhang, Y. Qiu, Z. Chen and X. Guo, *Corros. Sci*. 74 (2013) 71-82.
12. B. X. Huang, P. Tornatore and Y. Li, *Electrochimica Acta*. 46 (2000) 671-679.
13. T. Sasaki, R. Kanagawa, T. Ohtsuka and K. Miura, *Corros. Sci*. 45 (2003) 847-854.
14. T. Shibutani, Q. Yu, M. Shiratori and M. G. Pecht, *Microelectron. Reliab*. 48 (2008) 1033-1039.
15. D. Q. Yu, W. Jillek and E. Schmitt, *J Mater Sci: Mater. Electron*. 17 (2006) 229-241.
16. X. Zhong, G. Zhang, Y. Qiu, Z. Chen, X. Guo and C. Fu, *Corros. Sci*. 66 (2013) 14-25.
17. S. Zou, X. Li, C. Dong, K. Ding and K. Xiao, *Electrochimica Acta* 114 (2013) 363-371.
18. G. R. Meira, C. Andrade, C. Alonso, I. J. Padaratz and J. C. Borba, *Corros. Sci*. 50 (2008) 2724-2731.
19. G. R. Meira, C. Andrade, C. Alonso, I. J. Padaratz and J. C. B. Jr, *Atmos. Environ*. 41 (2007) 8431-8441.
20. P. Roberge, R. Klassen and P. Haberecht, *Mater. Des*. 23 (2002) 321-330.
21. Z. Cui, X. Li, K. Xiao and C. Dong, *Corros. Sci*. 76 (2013) 243-256.
22. ISO 9223, Corrosion of Metals and alloys, corrosivity of atmospheres classification, 1992.
23. S. Yee, R. A. Oriani and M. Stratmann, *J. Electrochem. Soc*. 138 (1991) 55-61.
24. A. Nazarova, M. G. Olivier and D. Thierry, *Prog. Org. Coat*. 74 (2012) 356-364.
25. H. N. McMurray, A. Holder, G. Williams, G. M. Scamans and A. J. Coleman, *Electrochimica Acta* 55 (2010) 7843-7852.
26. S W Zou, X G Li, C F Dong, H Y Li and K Xiao, *Acta Metall Sin*, 48 (2012) 687-695.
27. B. F. Dzhurinskii, D. Gati, N. P. Sergushin, V. I. Nefedov and Y. V. Salyn, *Russ J. Inorg. Chem+*. 20 (1975) 2307-2314.
28. G. T. Baronetti, S. R. Miguel, O. A. Scelza and A. A. Castro, *Appl. Catalysis* 24 (1986) 109-116.

29. T. Dieudonné, L. Marchetti , M. Wery, F. Miserque, M. Tabarant, J. Chêne, C. Allely, P. Cugy and C.P. Scott, *Corros. Sci*. 83 (2014) 234-244.
30. M. C. Biesinger, L. W. M. Lau, A. R. Gerson and R. S. C. Smart, Appl. Surf. Sci. 257 (2010) 887-898.
31. J. Haber, T. Machej, L. Ungier and J. Ziolkowski, *J. Solid State Chem*. 25 (1978) 207-218.
32. S. W. Gaarenstroom and N. Winograd, *J. Chem. Phys*. 67 (1977) 3500-3506.
33. T. L. Barr, *J. Vac. Sci. Technol*. A 9 (1991) 1793-1805.
34. Q. X. Li, Z. Y. Wang, W. Han and E. H. Han, *Corros. Sci*. 50(2008) 365-371.
35. B. Rosales, R. Vera and G. Moriena, *Corros. Sci*. 41 (1999) 625-651.
36. T. Kamimura, S. Hara, H. Miyuki, M. Yamashita and H. Uchida, *Corros. Sci*. 48 (2006) 2799-2812.
37. P. E. L. Moraes, R. J. Contieri, E. S. N. Lopes, A. Robin and R. Caram, *Mater. Charact*. 96 (2014) 273-281.
38. S. Chen, P. Wang and D. Zhang, *Corros. Sci*. 87 (2014) 407-415.
39. Y. L. Cheng, Z. Zhang, F. H. CAO, J. F. LI, J. Q. ZHANG, J. M. WANG and C. N. CAO, *Corros. Sci*. 46 (2004) 1649-1667.
40. E.B. Castro and C.A. Gervasi, *Int. J. Hydrogen Energ*. 25 (2000) 1163-1170.
41. J. A. Moreto, C. E. B. Marino, W. W. B. Filho, L. A. Rocha and J. C. S. Fernandes, *Corros. Sci*. 84 (2014) 30-41.
42. S. Zhang, A. Shrivastava, M. Osterman, M. Pecht and R. Kang, Electronic Packaging Technology & High Density Packaging, ICEPT-HDP, International Conference on, (2009) 116-122.
43. M. Sun, K. Xiao, C. F. Dong, X. G. Li and P. Zhong, *Acta Metall Sin* 47 (2011) 442-448.
44. Y. Xiang, Z. Wang, C. Xu, C. Zhou, Z. Li and W. Ni, *J. Supercrit Fluid* 58 (2011) 286-294.
45. M. Mori, K. Miura, T. Sasaki and T. Ohtsuka, *Corros. Sci.* 2002, 44(4): 887-898.
46. C. Lee, B. Nam, W. Choi, J. Lee, D. Choi and Y. Oh, *Mater. Lett*. 65 (2011) 722-725.
47. M. A. Amin and K. F. Khaled, *Corros. Sci*. 52 (2010) 1194-1204.
48. R. Solmaz, E. A. Sahin, A. Döner and G. Kardas, *Corros. Sci*. 53 (2011) 3231-3240.